

UC San Diego

UC San Diego Previously Published Works

Title

A probabilistic estimation approach for the failure forecast method using Bayesian inference

Permalink

<https://escholarship.org/uc/item/38m9j5v4>

Authors

O'Dowd, Niall M
Madarshahian, Ramin
Leung, Michael Siu Hey
[et al.](#)

Publication Date

2021

DOI

10.1016/j.ijfatigue.2020.105943

Peer reviewed

A PROBABILISTIC ESTIMATION APPROACH FOR THE FAILURE FORECAST METHOD USING BAYESIAN INFERENCE

Niall M. O'Dowd¹, Ramin Madarshahian¹, Michael Siu Hey Leung², Joseph Corcoran², and Michael D. Todd^{1,*}

¹ Department of Structural Engineering, University of California San Diego, 9500 Gilman Drive, La Jolla CA 92093-0085 USA; *email: mdtodd@eng.ucsd.edu

² Department of Mechanical Engineering, Imperial College London, UK

Key words: failure forecast method; Bayesian inference; fatigue life; remaining life estimation; structural health monitoring

Abstract. Positive-feedback mechanisms such as fatigue induce a self-accelerating behavior, captured by models displaying infinite limit-state asymptotics, collectively known as the failure forecast method (FFM). This paper presents a Bayesian model parameter estimation approach to the fully nonlinear FFM implementation and compares the results to the classic linear regression formulation, including a regression uncertainty model. This process is demonstrated in a cyclic loading fatigue crack propagation application, both on a synthetic data set and on a full fatigue experiment. A novel "switch point" parameter is included in the Bayesian formulation to account for nonstationary changes in the growth parameter.

1 Introduction

Information provided by structural health monitoring (SHM) data is generally used to assess the current diagnostic state of components or systems [1]. Such SHM assessments may be subsequently used to inform predictive models that estimate remaining useful life (RUL) or some related prognostic condition [2,3]. RUL is most commonly defined as the amount of time, subject to some assumed usage profile, that a structure has before achieving some limit state that prevents its ability to perform its intended design functions safely and reliably [4]. The achievement of this limit state (measured as time, response, or load cycles, or a similar metric) will be defined as the time-of-failure, denoted by the variable t_f .

In particular, this paper focuses on estimating t_f of specimens subjected to ultimate failure induced by fatigue cracking. A common method employed for predicting t_f in a fatigue scenario is the Paris-Ergodan crack growth law [5]. This law expresses the rate of crack growth as a function of parameters such as the stress intensity factor from the load around the crack tip, material properties which may be obtained experimentally, and stress information particular to the specific cyclic loading. Although motivated by linear elastic fracture mechanics, the parameters which affect t_f predictions using Paris' law have intrinsic uncertainty, and in fact they may be impossible to estimate or measure accurately in cases such as complex geometries, materials, or load states. Varying environmental effects may also infuse substantive uncertainty into the Paris' law approach.

Such uncertainties in Paris' law (and many other classes of such crack growth models) necessitated development of more probabilistic methods for estimating RUL in fatigue loading applications. Some of the sources of variability or uncertainty that affect prediction of t_f , generally regardless of modeling

39 approach, include (but aren't limited to) stochastic environmental or loading effects, uncertainty in
 40 initial material state, and measurement process noise. This inherently makes the prediction problem
 41 probabilistic, since typically these influences cannot be measured or estimated completely [6, 7]. One
 42 subsequent approach addressed this with a modified version of the Paris-Ergodan crack growth law
 43 known as the NASGRO equation, which quantified the material uncertainties and loading conditions in
 44 fatigue behavior using Monte Carlo (MC) analysis [8,9]. Mallor et al. recently presented a study on the
 45 probabilistic formulation for fatigue crack propagation based on the NASGRO equation and provided a
 46 stochastic approach for predicting statistical moments of fatigue lifetime for components subject to
 47 non-uniform loading patterns [10]. In this study, the RUL expected value and variance of numerically
 48 simulated fatigue loading experiments are approximated and verified using MC simulation. Artificial
 49 neural networks are also being used to estimate RUL, without the need for an explicit physical fatigue
 50 mathematical model form. Studies by Jimenez-Martinez et al. and Barbosa et al. show the results
 51 of using machine learning capabilities with only two inputs (component strain and fatigue cycle) to
 52 estimate failure [11,12]. Both studies reported a higher prediction capability at some load sequences in
 53 comparison to traditional modeling techniques.

54 For failure modes expected to possess self-accelerating observable behavior (such as unarrested
 55 crack growth), a method for estimating t_f that has been shown to have broad application is widely-
 56 known as the failure forecast method (FFM). Early origins of the FFM began with Fukuzono, who
 57 observed that landslide mechanics could be explained by using an empirical positive-feedback model of
 58 the inverse rate of ground strain [13]. Voight later formalized this observation into a more comprehensive
 59 predictive model and first coined the term "failure forecast method" [14,15]. The FFM has been further
 60 widely implemented in modeling a diverse variety of self-accelerating failure mechanisms, ranging from
 61 material-level failures (e.g., creep, fatigue) to volcanic eruptions [16–22]. This paper will focus on the
 62 use of the FFM to sample the distribution of t_f for fracture in fatigue loading applications. For fatigue
 63 cracking (and many other applications, for that matter), the FFM has traditionally been implemented
 64 in a linearized way by linearly regressing the inverse rate of crack growth against time, as detailed
 65 later in Section 2.1. When the inverse rate of the monitored feature approaches zero (the time axis
 66 intercept), the feature rate approaches infinity, and the failure event is defined to have occurred [16–18].
 67 However, the regression implementation of the FFM provides a single estimated point for t_f , which
 68 does not consider explicitly the propagation of uncertainty in the estimation process. A recent study
 69 proposed a model to approximate this propagated uncertainty in the FFM linear regression process [23];
 70 this same model will be used in this study to estimate probability density functions for t_f for the
 71 "classical" linear FFM approach, in comparison to the Bayesian model that will be proposed and
 72 implemented in this work. More recent work has shown that the linearity assumption made in the
 73 regression implementation of FFM has been observed to be false for both early and late stage crack
 74 growth [24]. This work shows that imposing linearity may cause a positive bias in t_f estimation for late
 75 stage crack growth, where the inverse feature rate has been observed to slope downward; this implies
 76 that the failure time occurs consistently sooner than predicted, introducing a non-conservative bias that
 77 could be catastrophic. While this study focuses on the problem of fatigue, a range of different damage
 78 mechanisms exhibit multiple distinct phases of progression determined by the underlying mechanics,
 79 and indeed the inclusion of pre-damage data will lead to non-constant trends, and so a solution to this
 80 problem will be widely applicable.

81 The Bayesian model introduced in this work allows both for relaxation of the linearity assumption
 82 and for sampling the posterior distribution of t_f . We shall compare t_f distribution models from the fully-
 83 Bayesian approach to t_f estimations made from the linear regression approach, including distributions
 84 from the linear regression uncertainty model. Approaching model parameter estimation from a Bayesian
 85 statistical perspective is advantageous when only a few realizations (or even a single realization) can be
 86 obtained for analysis, such as data from a single cyclic fatigue loading experiment. The operation of
 87 the Bayesian modeler consists of formulating and continuously sampling the distributions of model
 88 parameters as new data become available, intrinsically allowing for the generation of uncertainty
 89 distributions for each parameter, including t_f . We thus relax the linearity constraint by including a
 90 model parameter in the Bayesian-inferred parameter set which accounts for nonlinearity, rather than
 91 setting it to an assumed value.

92 Recent published works have begun to propose various uncertainty quantification approaches to
 93 the FFM. Commonly, published works operate on data from historic earthquakes, but the FFM is
 94 agnostic to the particular failure mechanism which makes these studies related to the current work.
 95 Bell et al. [25] evaluated the FFM using synthetic strain and earthquake sequences. A small amount
 96 of Gaussian noise was added to the strain rate data to simulate the effect of measurement error,
 97 and earthquake data was simulated as a Poisson process with mean rate and variance. The article
 98 synthesized 200 realizations of data for each process, and generated probability density functions
 99 based on t_f estimations of the FFM for each realization. Bevilacqua et al. [26] proposed a doubly
 100 stochastic enhancement of the FFM by introducing a formulation similar to the Hull-White model in
 101 financial mathematics. By including stochastic noise terms in the original FFM governing equation, t_f
 102 estimation uncertainty can be systematically characterized. Their method provides complete posterior
 103 probability distributions, allowing for worst case scenario estimation with a specified level of confidence.
 104 Bevilacqua's method is applied to earthquake eruption prediction, with small sets of data compared to
 105 the data presented in this study. In the domain of fatigue prediction, Leung et al. [24] compared the
 106 performance between conventional periodic inspections informing Paris' law parameters (themselves
 107 updated via Bayesian inference) and continuous monitoring for use by the linearized formulation of the
 108 FFM. In that study, random uncertainty in the damage accumulation rate measurements is the only
 109 source of uncertainty for the FFM, which in turn results in uncertainties in the regression fit and the
 110 extrapolated time axis intercept (t_f). The data are assumed to fit the model form, and it is assumed
 111 that data realizations are readily obtained.

112 While uncertainty modeling within the FFM has indeed progressed, the use of Bayesian inference
 113 is quite limited. Boue et al. in [20] and [27] implemented a Bayesian model to estimate the eruption
 114 time of volcanoes, specifically trained on data from Volcán de Colima. Their Bayesian model operated
 115 on the empirical power law which contained parameters including the failure time coinciding with
 116 eruption onset. Their Bayesian model generated confidence levels associated with the failure time,
 117 which is especially useful for crisis management and decision making. They showed that Bayesian model
 118 sampling methods were beneficial to exploring each measured feature, and using a linear regression
 119 for the FFM was not always relevant for every measured feature set. The present work provides a
 120 significantly broader look into the use of Bayesian reasoning in the FFM, achieved by evaluating the
 121 performance of the Bayesian model on synthetic data with varying parameters, allowing for many
 122 realizations to be generated. We also provide advancement by developing a parameter switching model

123 which determines a discrete point where our Bayesian parameters can switch (detailed in section 4).

124 Within the FFM framework, this paper compares two probabilistic models for estimating t_f : the
 125 linear regression with an uncertainty model, and the proposed fully-Bayesian approach. The probability
 126 density functions (PDFs) of the linear regression model $p(\hat{t}_f)$ and the t_f posterior belief distributions of
 127 the Bayesian model are compared on a synthesized dataset (in section 3), and a real fatigue dataset (in
 128 section 4).

129 2 Predictive Models

130 The most common general FFM model form proposes that the time rate-of-change R of some
 131 time-dependent measured feature Ω , $R = \dot{\Omega}$, obeys the following evolution equation

$$\dot{R} = kR^\alpha, \quad (1)$$

132 where $k > 0$ and $\alpha > 1$ are empirical constants relevant to the specific physical process. As these
 133 constants are not derived from a mechanics consideration, one attractive property of the FFM model
 134 formulation is that, unlike Paris' law, no knowledge of application-specific loading parameters and
 135 material properties is required. The solution to Eq. (1), assuming that the rate R at the time of
 136 failure t_f is R_f (often assumed infinite in the original literature, since the model form admits an infinite
 137 asymptote at t_f) is given by

$$R(t) = [R_f^{1-\alpha} + k(\alpha - 1)(t_f - t)]^{\frac{1}{1-\alpha}}. \quad (2)$$

138 The FFM literature have shown it to be more convenient to consider the *inverse* of the rate R , since
 139 this facilitates easier definition of the failure criterion, i.e., the inverse rate tending to zero rather than
 140 the rate itself tending to infinity at the time of failure. Defining the inverse rate $P = R^{-1}$, the solution
 141 Eq. (2) becomes

$$P(t) = [P_f^{\alpha-1} + k(\alpha - 1)(t_f - t)]^{\frac{1}{\alpha-1}}, \quad (3)$$

142 where t_f may be solved for as

$$t_f = t + \frac{P^{\alpha-1} - P_f^{\alpha-1}}{k(\alpha - 1)}. \quad (4)$$

143 This form of the FFM predicts that failure will occur at some inverse feature rate-informed amount of
 144 time after present time t , encapsulated in the second term on the right-hand side of Equation 4.

145 2.1 The Linearized FFM with Linear Regression Method

146 The linearized FFM approach is to assume that α is approximately 2 (based on a number of
 147 empirical studies done over a variety of failure mechanisms, as evidenced in the literature already cited),
 148 which permits a linear regression on Eq. (4), after rearrangement, as

$$P - P_f = kt_f - kt. \quad (5)$$

149 Clearly, as $t \rightarrow t_f$, then $P \rightarrow P_f$, where the mathematically idealized target failure criterion is that
 150 $P_f = 0$, corresponding to $R_f \rightarrow \infty$, as alluded to above. By setting it to any positive value, a degree
 151 of conservatism is introduced into the approach. Of course, in most practical applications, “failure”
 152 occurs at a point prior to an infinite data rate-of-change observation, but to be consistent with general
 153 implementation in the literature and for the purposes of parametric studies in this paper, we will
 154 employ $P_f = 0$ as the failure criterion, which won’t change the basic nature of this study. With that,
 155 the two regression coefficients obtained from a time/data linear regression (over some given window of
 156 time) are given by $\beta_0 = kt_f$ (intercept) and $\beta_1 = -k$ (slope) such that the regression-estimated time
 157 to failure is $\hat{t}_f = -\beta_0/\beta_1$, the negative of the ratio of the intercept to the slope. If k is not known, it
 158 could be estimated via a maximum likelihood technique or via Markov Chain Monte Carlo (MCMC)
 159 sampling methods [22, 28].

160 We will review the uncertainty model recently developed for this linear regression process presented
 161 in detail in [23, 24]. Any given regression on some time-stamped feature set represents a single “block”
 162 observation, which is presumed representative of an ensemble population of regressions over the same
 163 time frame. Thus, the regression coefficient vector $\beta = [\hat{\beta}_0, \hat{\beta}_1]^T$ is an estimate from populations of
 164 regression coefficients. A visualization of this process is seen in Figure (1).

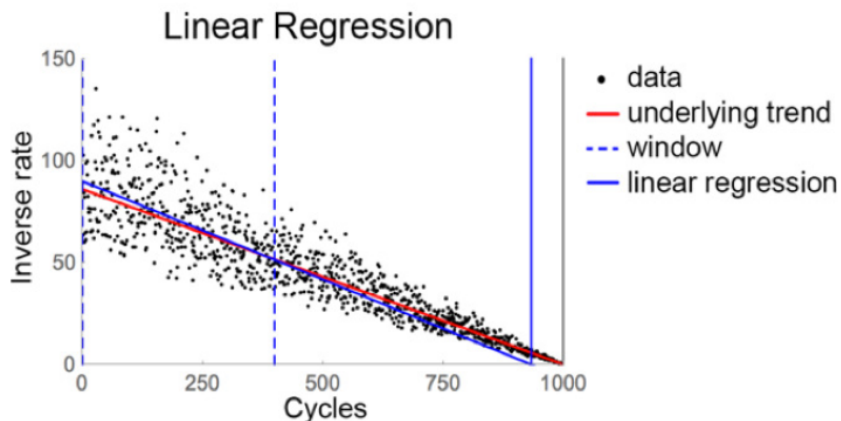


Figure 1: An example of a regression block occurring at 300 cycles. The vertical solid line represents the failure point.

165 For a given linear regression model $\mathbf{P} = \mathbf{X}\beta + \mathbf{e}$, where \mathbf{P} are observations of data, \mathbf{X} is the
 166 design matrix, and \mathbf{e} are the residuals between the data the linear regression model. It is assumed
 167 that the regression process yields residuals that are unbiased, uncorrelated, and normally-distributed
 168 $\mathbf{e} \equiv N(\mathbf{0}, \sigma^2 \mathbf{I})$, under typical central limit theorem assumptions (regardless of the distribution of the
 169 regressed data, \mathbf{P}). Under this assumption, the theory follows that the regression coefficients themselves
 170 have normal distributions $\hat{\beta}_j \equiv N(\beta_j, \sigma^2 (\mathbf{X}^T \mathbf{X})^{-1})$, $j = 0, 1$, and the superscript "T" indicates the matrix
 171 transpose. An unbiased estimate of the population error variance is $\sigma^2 = \|\mathbf{P} - \mathbf{X}\hat{\beta}\|^2 / (n - 2)$, where
 172 n is the number of data points used in the regression design, reduced by two since two regression
 173 coefficients were estimated in the process. Given the uncertainty models in the regression coefficients,
 174 the time-of-failure is predicted by $\hat{t}_f = -\hat{\beta}_0/\hat{\beta}_1$, as stated previously. The distribution of this ratio of

175 *correlated* normal variables may be computed as

$$p(\hat{t}_f) = \int_{-\infty}^{\infty} \frac{p(-\hat{t}_f \hat{\beta}_1, \hat{\beta}_1)}{|-1/\hat{\beta}_1|} d\hat{\beta}_1 \quad (6)$$

176 where $p(\hat{\beta}_0, \hat{\beta}_1)$ is the bivariate normal density function. The computation of Eq. (7) yields the result

$$p(\hat{t}_f) = \frac{\sqrt{1-\rho^2} \sigma_0 \sigma_1 e^{-\frac{-\mu_1^2 \sigma_0^2 + 2\rho\mu_0\mu_1\sigma_0\sigma_1 - \mu_0^2 \sigma_1^2}{2\sigma_0^2 \sigma_1^2 (1-\rho^2)}}}{\pi(\sigma_1^2 + 2\rho\sigma_0\sigma_1\hat{t}_f + \sigma_0^2\hat{t}_f^2)} + \frac{e^{-\frac{(\mu_1 + \mu_0\hat{t}_f)^2}{2(\sigma_1^2 + 2\rho\sigma_0\sigma_1\hat{t}_f + \sigma_0^2\hat{t}_f^2)}} \operatorname{erf}\left(\frac{\mu_1\sigma_0(\rho\sigma_1 + \sigma_0\hat{t}_f) - \mu_0\sigma_1(\sigma_1 + \rho\sigma_0\hat{t}_f)}{\sqrt{2-2\rho^2}\sigma_0\sigma_1\sqrt{\sigma_1^2 + 2\rho\sigma_0\sigma_1\hat{t}_f + \sigma_0^2\hat{t}_f^2}}\right)}{\sqrt{2\pi}(\sigma_1^2 + 2\rho\sigma_0\sigma_1\hat{t}_f + \sigma_0^2\hat{t}_f^2)^{3/2}}, \quad (7)$$

177 where erf^* is the error function, $\mu_j = \hat{\beta}_j$, $\sigma_j = \sqrt{\|\mathbf{P} - \mathbf{X}\hat{\beta}\|^2 (\mathbf{X}^T \mathbf{X})_{j+1,j+1}^{-1} / (n-2)}$, and $\rho =$
 178 $\|\mathbf{P} - \mathbf{X}\hat{\beta}\|^2 (\mathbf{X}^T \mathbf{X})_{12}^{-1} / (\sigma_0\sigma_1(n-2))$, with $j = 0, 1$; the double subscript 1,2 refers to the row-column
 179 selection of the subscripted matrix. Strictly speaking, since the exact population μ_j and σ_j are not
 180 known *a priori* and must be estimated from the data as presented above, a sampling distribution for
 181 the ratio mean and standard deviation should be derived, but here the population ratio distribution,
 182 Eq. (7) will be used as a surrogate. It should be noted that this PDF has no analytically-calculable
 183 order statistics [29]. However, Refs. [23] and [24] used Eq. (7) and showed it was sufficient to describe
 184 the distribution of the failure time, and it will be used here.

185 2.2 Bayesian Model

186 At its core, the Bayesian technique operates by continuously updating posterior beliefs (dis-
 187 tributions) of parameters as new data become available. The general form of Bayes' equation is

$$p(\Theta|D) = \frac{P(D|\Theta) \times P(\Theta)}{P(D)}, \quad (8)$$

189 where D represents the data (in this case we are using inverse crack growth rate data, or P) and Θ
 190 represents the model parameters to be estimated (akin to the regression coefficients of the previous
 191 section). After obtaining new data, denoted by $D = \{d_1, \dots, d_n\}$, model parameter beliefs are updated,
 192 $P(\Theta|D)$, influenced by the likelihood $P(D|\Theta)$ and a prior distribution, $P(\Theta)$. This prior distribution
 193 describes the modeler's degree of belief about the parameter values before observing any data, which
 194 may also be based on past experience, if such experience exists. One can also use uninformed prior
 195 distributions, e.g., a Jeffery's prior, if no such prior belief or information exists.

196 In the current work, the parameter vector Θ consists of the parameters k , α , t_f , and the standard
 197 deviation σ_l (noise parameter) that will be a part of our likelihood function (discussed more later).
 198 Because t_f should be positive and greater than the current time of data collection t , the prior is assumed
 199 to be uniformly distributed from current time, t , to ∞ . The prior for k is also assumed to be an
 200 improper (it doesn't integrate to unity) uniform distribution, from 0 to ∞ because it is known to be
 201 positive. We chose the prior for α to be uniform between 1.5-2.5 because the literature shows that this
 202 parameter is close to 2 (as per the discussion above leading to the linear regression implementation)

203 and fluctuates in accordance to physical properties of failure mechanisms [22]. We chose the prior for
 204 σ_l to be half normal, a weakly informative distribution as suggested by Gelman et al. [30,31]. Table (1)
 205 shows a summary of the priors selected for the parameters.

Table 1: Parameters of the Bayesian model (synthetic data)

Parameter	Prior
t_f	Improper uniform distribution with lower bound of t
k	Improper uniform distribution with lower bound of 0
α	Uniform distribution between 1.5 and 2.5
σ_l	Half normal distribution, standard deviation of 1

206 If a specific forward measurement model were proposed or developed, a tailored likelihood function
 207 could be derived from that. The current work, however, seeks to maintain a Bayesian model that is
 208 more agnostic to the specific kind of data/features D that are used, so a normal model for the likelihood
 209 function $N(\mu_l, \sigma_l)$ was chosen. In order to capture the heteroscedastic converging effect of the noise
 210 structure observed in real fatigue experiments [22, 24], inference is performed in the logarithmic space,
 211 i.e., $P(D'|\Theta) = N(\mu_l, \sigma_l)$ where $D' = \log(D)$. In the logarithmic space, the noise statistics observed
 212 on inverse feature rate data can be approximated as stationary which allows the Bayesian model to
 213 sample the noise standard deviation consistently. By using inference in the logarithm domain, and
 214 maintaining the sampling of the likelihood's standard deviation σ_l outside the logarithm domain, we
 215 were able to capture posterior predictions matching the noise structure, seen in Figure (4). The mean
 216 of our likelihood function μ_l takes the form of the logarithm of Eq. (7), containing sampled parameters
 217 α , k , and t_f , provided by

$$\mu_l = \log([P_f^{\alpha-1} + k(\alpha-1)(t_f-t)]^{\frac{1}{\alpha-1}}), \quad (9)$$

218 where t is current time, and $P_f = 0$ remains the failure criterion; thus our likelihood function may be
 219 written

$$P(D'|\Theta) = \frac{1}{\sqrt{2\pi}\sigma_l} e^{-\frac{\left(D' - \log([P_f^{\alpha-1} + k(\alpha-1)(t_f-t)]^{\frac{1}{\alpha-1}})\right)^2}{2\sigma_l^2}}, \quad (10)$$

220 Obtaining the analytical expression for the joint posterior of parameters requires calculating
 221 high dimensional integrals, which is not often feasible. In the present case, the Bayesian model is
 222 of dimension 4, making sampling-based algorithms like Markov chain Monte Carlo (MCMC) viable
 223 to explore the posterior belief space. Sampling-based methods such as MCMC are an absolutely
 224 fundamental part of Bayesian inference, as they allow the design of more flexible and complex models
 225 of higher dimension. In the current work, we used the No-U-Turn Sampler (NUTS) within the PyMC3
 226 python package [32] to sample the joint posterior of parameters. The NUTS sampler is an extension to
 227 the Hamiltonian Monte Carlo (HMC) algorithm which eliminates the need to manually select a desired
 228 number of steps and their size. NUTS works by building a set of likely candidate points spanning a
 229 wide range of the target distribution and stopping when the selection begins to double back on itself.
 230 We have made this selection because NUTS retains (and in some cases improves upon) HMC's ability
 231 to generate effectively independent samples efficiently [33]. The initialization method of the sampler
 232 was selected as the "jitter+adapt_diag" option built into the PYMC3 package, which worked by setting
 233 the starting point of the Bayesian sampler with a identity mass matrix, adapting a diagonal based on

234 the variance of the tuning samples, and adding a uniform "jitter" in $[-1, 1]$ to the starting point of each
 235 chain, detailed in [32]. We used 2 chains for each simulation to verify convergence.

236 To generate posterior predictions using observable data, our model utilizes predictive inference,
 237 which is derived from the general form of the Bayesian model. After observations have been recorded
 238 in D' ($D' = \log(D)$), we can predict an unknown observable, \tilde{D}' , using similar Bayesian logic. The
 239 distribution of \tilde{D}' is called the posterior predictive distribution, and is shown Eq. (11), where the last
 240 step follows the assumed conditional independence of \tilde{D}' and D' given Θ . Figure (2) shows examples of
 241 the posterior predictive distributions at two separate cycle instances [30].

$$\begin{aligned} p(\tilde{D}'|D') &= \int p(\tilde{D}'|\Theta, D')p(\Theta|D')d\Theta \\ &= \int p(\tilde{D}'|\Theta)p(\Theta|D')d\Theta \end{aligned} \quad (11)$$

242 To mimic the nature of failure prognosis, parameter estimations were performed by using data
 243 from a time window containing all sample points until the present cycle. This is seen in Figure (2)
 244 where data projections from the Bayesian model are generated based on data from the first cycle to the
 245 current cycle. The posterior predictions seen in figure (2) are made from synthesized data described in
 246 a subsequent section.

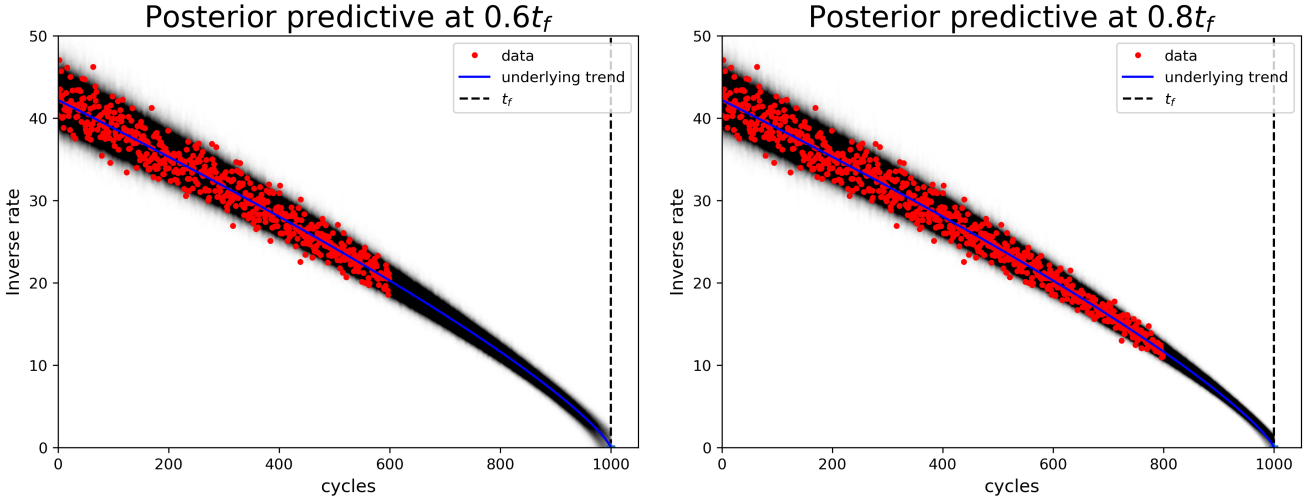


Figure 2: Predictions generated by the Bayesian model at different time windows. Figures show prediction at $0.6t_f$ (left) and $0.8t_f$ (right). Red dots show the inverse feature rate data, the black shaded regions show the posterior prediction.

247 Figure (2) shows a progression of the predictive capabilities of both models. The data on each plot
 248 (red points) show the data D provided to the Bayesian model (before transformation into log-space D').
 249 The posterior prediction made by the model is shown in the shaded regions. Darker shaded regions
 250 on the plot show areas of where the posterior predictive generated more samples, corresponding to
 251 areas of higher probability of data. The heteroscedastic (appears to converge) nature of the noise of
 252 the prediction areas in the plots is a result of the logarithm space mean likelihood μ_l sampling with a
 253 "non-logarithm" space sampling of the likelihood standard deviation σ_l .

254 We verified the Bayesian model's posterior prediction and the linear regression model's uncertainty
 255 PDF against a Monte-Carlo brute force simulation taken from simulated data at different cycles,

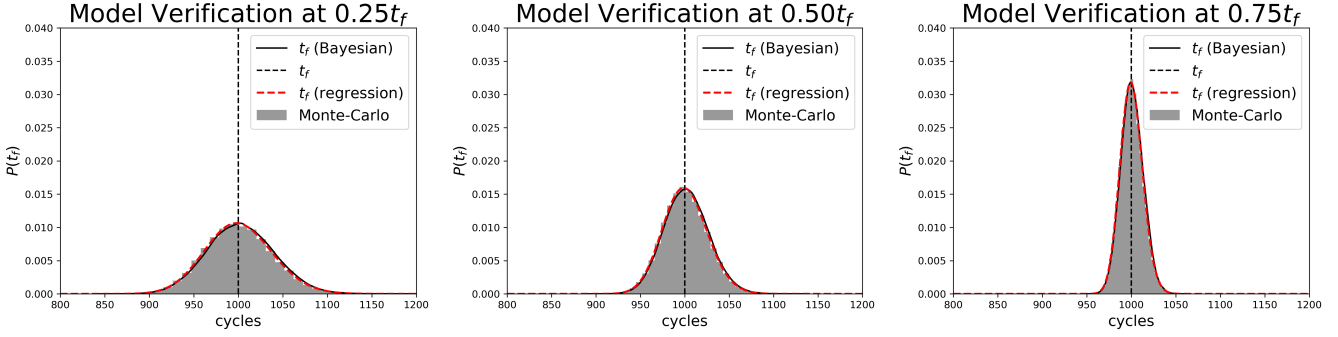


Figure 3: Verification of the agreement of the Bayesian posterior predictions of t_f , the linear regression uncertainty model, and a brute-force Monte-Carlo simulation, taken at different cycles.

256 corresponding with $0.25t_f$, $0.50t_f$, and $0.75t_f$. For the simplest case, in each verification in Figure (3)
 257 we assumed $\alpha = 2$ (thus not initially considered part of the Bayesian hyperparameter set), and sampling
 258 occurring at a known, prescribed time t . Figure (3) shows $p(t_f)$ provided by the linear regression
 259 uncertainty model in Eq. (7), the posterior distribution of t_f obtained from the Bayesian model, and
 260 a Monte-Carlo brute force simulation using Eq. (3) with noise added to the P_f term. We observed
 261 excellent agreement in this baseline verification process, which allows us to directly compare the two
 262 models' estimation capabilities.

263 We will next look at comparisons between the linear regression t_f and the Bayesian model posterior
 264 predictions of t_f using synthesized data based a fatigue experiment and then unaltered data from a
 265 real fatigue experiment.

266 3 Synthesized Fatigue Data Experiment

267 A fatigue test was simulated based on a laboratory-scale accelerated fatigue test as described in
 268 Corcoran [22]. Inverse strain rate data and time (fatigue cycles) were scaled to facilitate easier evaluation
 269 of Eq. (7), as the actual values from the test made numerical evaluation of Eq. (7) challenging. Data
 270 were generated at each fatigue cycle N , $0 < N < 1000$, where the actual time of failure from [22]
 271 was scaled to $t_f = 1000$ cycles, using Eq. (3). Such simulations were conducted at three different
 272 uncertainty/noise levels (0.02, 0.05, and 0.10), where the noise on the data P were assumed unbiased
 273 lognormal, i.e., the logarithm of the noise was normally-distributed with stationary zero mean and
 274 variance σ^2 . Practically, the noise-free data was generated using Eq. (3) and normally distributed noise
 275 was added to the logarithm of the noise-free data. The resulting data was then transformed back into
 276 "non-logarithm" space to be used as the available data for both the linear regression model and the
 277 Bayesian model. This procedure was used to generate a noise structure which mimics the trend of the
 278 real accelerated fatigue test from [22]. Figure (4 top left) shows the feature rate, $R(N)$ from Eq. (2),
 279 and figure (4 top right) shows inverse feature rate, $P(N)$ from Eq. (3) for a synthetic data realization
 280 where $\alpha = 1.75$. Figure (4 bottom left) shows the feature rate, $R(N)$ from Eq. (2), and figure (4 bottom
 281 right) shows inverse feature rate, $P(N)$ from Eq. (3) for a synthetic data realization where $\alpha = 2.25$. It
 282 is apparent that the α parameter is responsible for the convexity/concavity of the inverse feature rate,
 283 and can cause substantial errors in t_f (x-intercept) estimation due to nonlinearity when $\alpha \neq 2$.

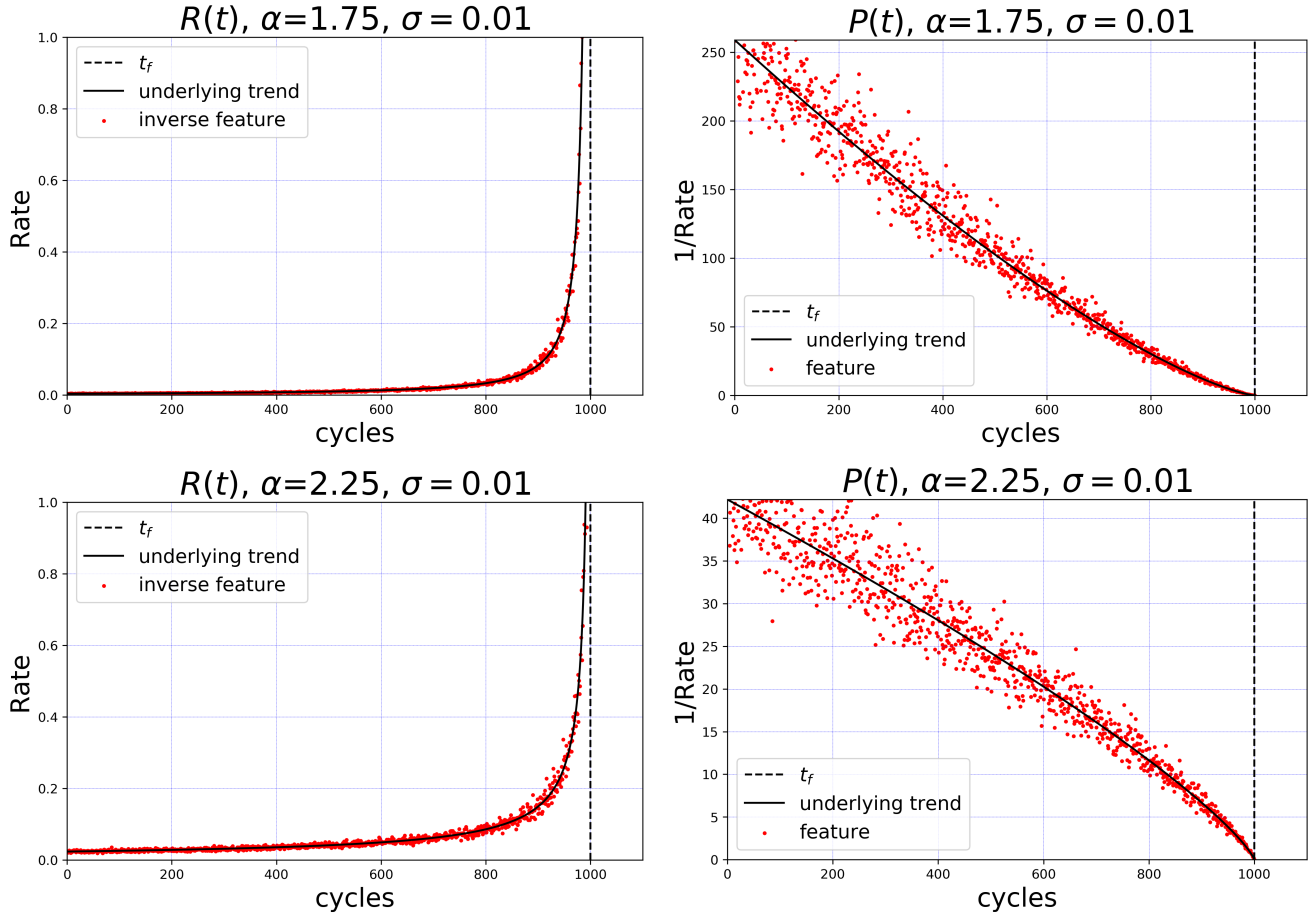


Figure 4: Realizations of simulated data with $\alpha = 1.75$ (top) and $\alpha = 2.25$ (bottom). Left plots show the feature rate (Eq. (2)), and right plots show the inverse feature rate (Eq. (3)). The linear regression and Bayesian model operated on the inverse feature rate (right plots).

284 3.1 Results

285 This section includes the results of t_f (regression) and t_f (Bayesian) on synthetic data with a
 286 variety of σ and α values: $\alpha = 1.75 - 2.25$, $\sigma = 0.02 - 0.10$. Estimations are taken with the entirety
 287 of the data until the current time without windowing, i.e. the $0.4t_f$ distribution represents using the
 288 first 40% of the data before failure. Each plot in figure (5) shows the evolution of t_f (Bayesian) and t_f
 289 (regression), for cycles $0.4t_f$ to $0.9t_f$. Figure (6) shows $t_f - \alpha$ joint distributions made by the Bayesian
 290 model.

291 When $\alpha < 2$, as seen in figure (5, top row), the shape of the inverse feature rate is convex, or
 292 curving upward along the horizontal axis, as seen in figure (4), as often observed in stage 1 crack
 293 growth [22]. Figure (5, top row) shows t_f (Bayesian) and t_f (regression) from data generated where
 294 $\alpha = 1.75$. The nonlinear inverse feature rate governed by $\alpha < 2$ causes t_f (regression) to greatly
 295 underestimate t_f for all levels of noise (with tight distributions), due to the linear regression model's
 296 forced linearity assumption of the inverse feature rate. Distributions of t_f (Bayesian) are able to
 297 include nonlinear inverse feature rate effects, which allows the distributions to converge onto the true
 298 t_f value, shown in t_f distributions at cycles $0.8t_f$ and $0.9t_f$ for all noise levels. In all noise cases, t_f
 299 (Bayesian) followed a trend of negatively biased, conservative estimations in prediction cycles $0.4t_f$ to
 300 $0.6t_f$, then providing a positive bias in the estimation at cycle $0.7t_f$, before centering onto the true

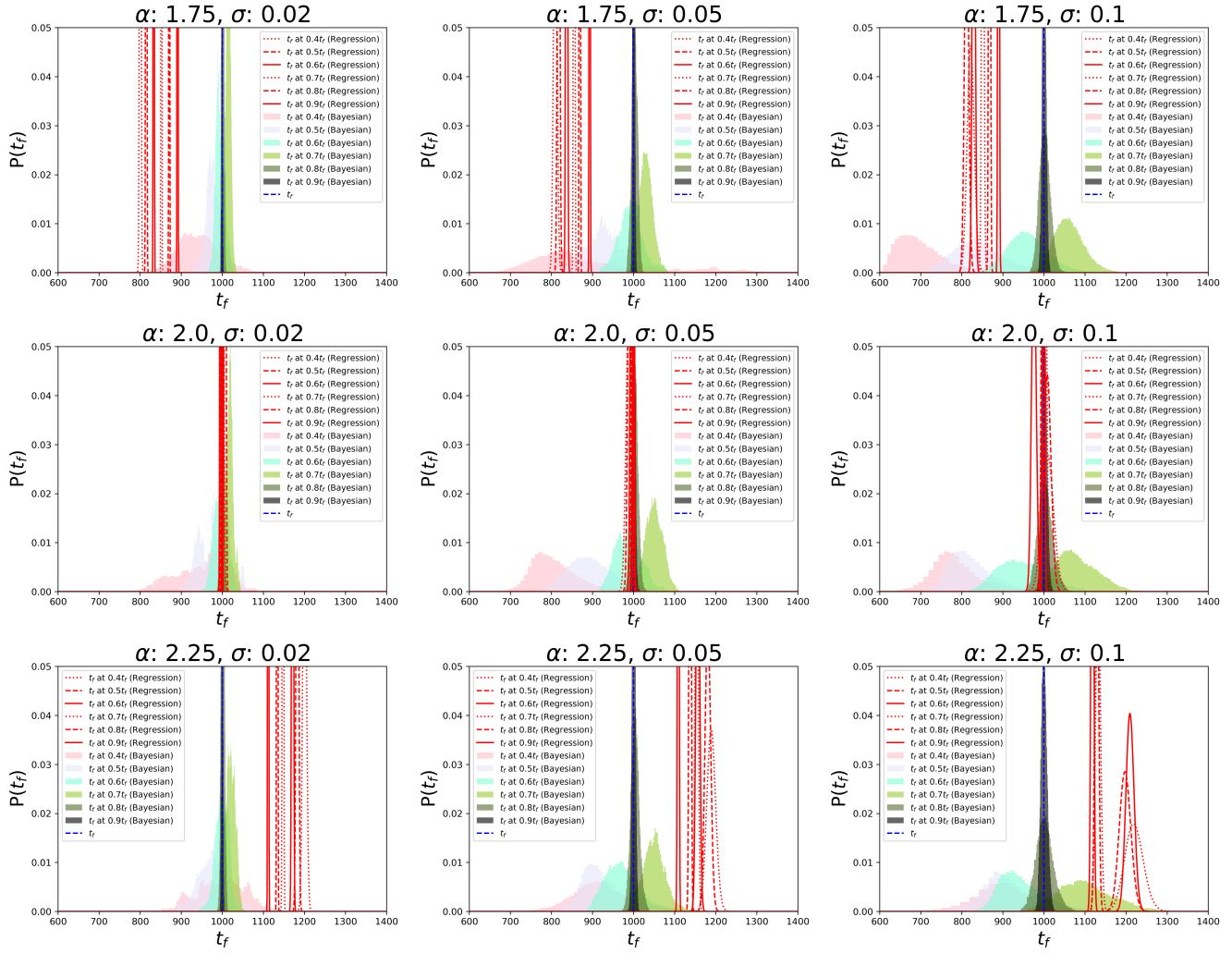


Figure 5: t_f (Bayesian) compared to t_f (regression).

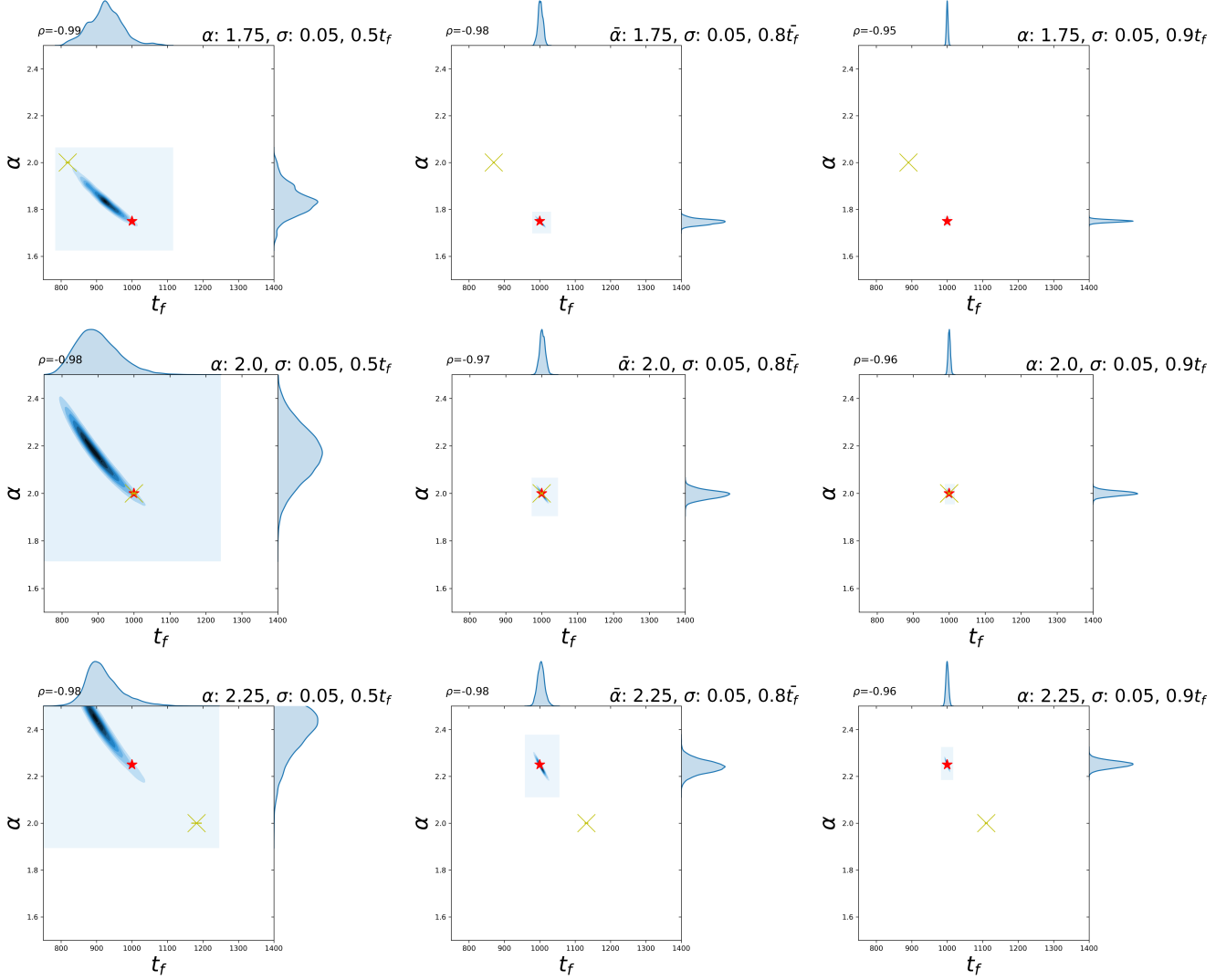


Figure 6: Joint Distributions of t_f and α distributions sampled by the Bayesian model. The yellow \times is the median prediction of the linear regression model, with an error bar extending to \pm the standard deviation of a best-fit normal distribution (not always visible in the figure due to their very small extent from the prediction), the blue shaded regions correspond to the Bayesian model's joint traces, and the red \star is the true value of α and t_f . The linear regression marker is not estimating the value of α , and is intrinsically set at 2.0.

301 t_f for prediction cycles $0.8t_f$ and $0.9t_f$. In the smallest noise case $\sigma = 0.02$, all of the sampled t_f
 302 distributions included the true t_f . As expected, as more data became available to the Bayesian model,
 303 t_f (Bayesian) distributions showed increased confidence (reduced variance). In the medium and large
 304 noise cases, $\sigma = 0.05$ and $\sigma = 0.1$, early cycle predictions were too negatively biased to incorporate the
 305 true t_f until prediction cycles at $0.5t_f$ and $0.6t_f$, respectively.

306 One circumstance where the linear regression model outperformed the Bayesian model is when
 307 $\alpha = 2$, as seen in figure (5, middle row) as observed in stage 2 crack growth; this is because the
 308 linear regression model assumes the inverse feature rate is linear, while the Bayesian model samples
 309 α , (nonlinearity measure), unlike during the model verification in figure (3). For noise level $\sigma = 0.02$,
 310 t_f (Bayesian) incorporated t_f at each prediction cycle, but with considerably less confidence than t_f
 311 (regression). The Bayesian model, performed similarly as the $\alpha = \{1.75, 2.25\}$ cases, with increasing
 312 levels of negative bias as noise σ level increases, and being positively biased at cycle $0.7t_f$. The value
 313 of t_f (Bayesian) converged to the true t_f value at cycles $0.8t_f$ and $0.9t_f$ for all σ levels.

314 Simulations run using data realized with $\alpha > 2$, also caused considerable bias in t_f (regression),
 315 seen in figure (5, bottom row). As observed in stage 3 crack growth, when $\alpha > 2$ the shape of the
 316 inverse feature rate is concave, or curving downward along the x-axis, as seen in figure (4). The linear
 317 regression is based on assuming the linearity of the inverse feature rate causing t_f (regression) to be
 318 positively biased for all levels of noise. This equates to earlier-than-predicted failure, which may be
 319 undesirable from a practical standpoint. The Bayesian model was able to adapt to the nonlinear inverse
 320 feature rate, and t_f (Bayesian) distributions behaved similarly to the distributions on data realized
 321 with $\alpha = 1.75$ and $\alpha = 2.0$. The Bayesian t_f predictions had increasing levels of negative bias as noise
 322 σ level increased, but t_f (Bayesian) shown to converge onto the true t_f value by $0.8t_f$ for all cases.

323 In summary, in all noise levels σ and α parameters, The Bayesian model was observed to converge
 324 to include the true t_f as the prediction cycle increased. The Bayesian model performed agnostic to the
 325 true value of α , while the bias of the linear regression estimator was determined by α .

326 A sample of α - t_f parameter joint distribution plots generated with the Bayesian model are shown
 327 in figure (6). Darker regions in each plot correspond to areas containing more samples meaning higher
 328 probability estimates from the Bayesian model. The distributions on the outside of the plot grid
 329 represent the sampled distribution of t_f (bayesian) (top of each plot) and α (right of each plot). The
 330 star on each plot shows the exact t_f and α values. The \times shows t_f (regression), which is constrained to
 331 $\alpha = 2$, with an error bar extending to $+/-$ the standard deviation of a best-fit normal distribution. It
 332 should be noted that no correlation was assumed for α and t_f in the prior beliefs, but a highly negative
 333 correlation is observed in the joint posterior distribution. For every simulation, we observed a strong
 334 negative correlation ($\rho \approx -0.95$ to -0.99) between the sampled α and t_f parameters, suggesting a
 335 next-iteration Bayesian model could incorporate a joint α - t_f distribution, or the possibility of combining
 336 terms to simplify the average term in the likelihood taken from Eq. (3) through principal component
 337 analysis.

338 Of course, the bias evident in the linear regression may be addressed by non-linear regression and
 339 solving for α , in addition to k and t_f , as shown in [22]. The benefit of using the Bayesian approach
 340 over non-linear regression is that it provides a full probabilistic analysis, is useful for exploring the
 341 distributions of all parameters (seen in figure 6), and may be built on to include more complexity as
 342 shown in the following section.

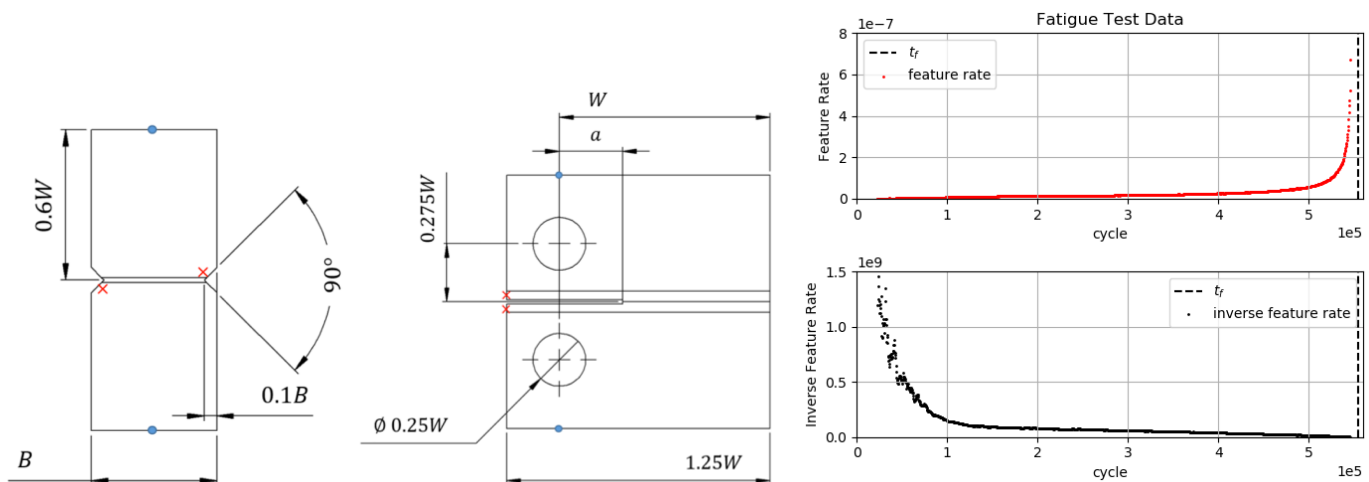


Figure 7: Left and center show geometry of the specimen used in the fatigue experiment. Right shows feature (crack growth rate) and its inverse with respect to cycle.

4 Fatigue Data Experiment

To further evaluate the Bayesian model, we performed failure prediction on another set of data from a fatigue experiment, first published in [24], again using an input feature related to inverse crack growth. This experiment differed from the first experiment presented in Section 3 because the fatigue data was used directly here, without bootstrapping or adjusting levels of noise or the α parameter. The motivation for this experiment was to test our Bayesian model on unaltered data and fully challenge the usual FFM assumptions on stationarity. The feature data was taken from a fatigue experiment using a standard 316 stainless steel compact tension test specimen, detailed in figure (7) and Tables (2) and (3). The feature was monitored using a permanently-installed potential drop measurement system, and the results plotting the rate of normalized resistance (related to crack growth through a simple polynomial) as a function of fatigue cycle are shown in figure (7, right), which also shows the inverse rate of normalized resistance [34]. The measurement in this experiment contains observations throughout the entire crack propagation event, potentially including crack growth stages 1-3, which is shown to correspond to a transient, unknown α [22, 24]. The failure mechanism of the experiment was ductile fracture, making the selection of the exact t_f cycle non-trivial. The potential drop system was removed at cycle 545,455, when the coupon began to exhibit a narrowing of cross-section (necking), and the specimen was removed from the fatigue testing machine at cycle 555,000 before complete fracture. We chose to express the actual t_f as a range between cycle 545,455 and 565,455.

Table 2: Fatigue test specimen dimensions

Parameter	Value
W (mm)	50
B (mm)	25
a (mm)	15.5
Maximum Load, P_{max} (kN)	11
Load Ratio, R (-)	0.1

The non-stationary nature of α (nonlinearity measure) in the real, unaltered fatigue test caused an influential difference compared to the synthesized data which was generated with a constant α value.

Table 3: Quantified uncertainties of each input parameter of the empirical crack growth law.

Parameter	Mean Value	Standard Error
Measured Crack Length, a_0 (mm)	Updates with each inspection	1
Critical Crack Length, a_f (mm)	38	Not considered
Paris Constant, $\ln(C)$	-25.5	0.264
Paris Exponent, m	2.88	Not considered
Maximum Load, P_{\max} (kN)	35	3.5
Load Ratio, R	0.1	Not considered
Geometry, $Y(a)$	Calculated from standards	Not considered

363 Performing Bayesian inference on the entire series of data (which may include multiple stages of crack
364 growth) can introduce biased estimation due to the non-stationarity of parameters. Standard practice
365 of implementing the FFM often includes truncating the visibly nonlinear inverse feature rate data,
366 which can introduce human error influenced by where the user chooses to truncate. To mitigate the
367 effects of this potential bias and subjectivity, we designed a method to truncate data estimated to be
368 recorded during different-than-current crack growth stages. We utilized PYMC3 to develop a Bayesian
369 model that incorporates two distinct, uncorrelated sets of Θ (all of the sampled parameters) determined
370 by a switch point selected by the maximum posterior belief of a sampled α switch point parameter
371 (noted as α_{sp}), i.e. completely separating the sampled parameters after a discrete cycle where α has
372 is estimated to change, signifying the change in crack growth stage. Though crack growth has been
373 observed to have 3 stages, our model allowed for only 2 sets of Θ because the model provided poor
374 results when a second switch point (3 stage model) was introduced; we hypothesize that this is due
375 to a relatively low amount of data in the third crack growth stage. This α -switching model used the
376 same likelihood function (Eq. (10)) as the previously proposed model, with slightly altered Θ priors,
377 summarized in Table (4). Due to previous literature showing that crack growth after stage 1 exhibits
378 $\alpha \geq 2$ behavior [22, 24], the prior selected for the second α parameter was constrained to a uniform
379 distribution from 2.0 to 2.2. The prior selected for the α_{sp} parameter was a uniform distribution from
380 0 to current time t .

381 Figure (8) shows the results of the α -switching model compared to t_f (regression) estimations
382 using full and truncated data sets. For current cycle= $\{0.55t_f, 0.65t_f, 0.75t_f, 0.98t_f\}$, the Bayesian
383 model consistently estimated α_{sp} to have a posterior distribution with a mean cycle of approximately
384 112,300, around 20% through the experiment, shown on each plot. The dashed line shows the t_f
385 (regression) using the full test data including stage 1 crack growth, which greatly underestimates the
386 actual t_f for every estimation cycle. We also chose to show t_f (regression) using only data after the
387 Bayesian-estimated α_{sp} cycle, which improved estimation, but still yielded negatively biased results for
388 cycles $0.55t_f$ - $0.57t_f$, and overestimated the actual t_f for cycle $0.98t_f$. We attribute the underestimation
389 to the selection of the α_{sp} ; the α -switching model selected what appears to be the inflection point of
390 the data, leaving some nonlinear data remaining after truncation. The overestimation of the truncated
391 t_f (regression) at $0.98t_f$ may be due to the inverse feature rate's nonlinear behavior at later fatigue
392 cycles. In implementation, we hypothesize that t_f (regression) would benefit from truncating data from
393 a later cycle. The Bayesian α -switching model was able to provide more accurate t_f estimations which
394 were able to include the actual t_f range for all cycle predictions, and we saw our model converging
395 towards the normal distribution as more data was made available. The interval of the actual t_f was

396 represented in high density regions of each (Bayesian) t_f PDF, with high accuracy in cycles past $0.65t_f$.
 397 The α -switching Bayesian model was able to objectively provide a distribution for the crack stage
 398 growth transition cycle, improving the accuracy of t_f (regression) when using truncated data, while
 399 also providing highly accurate (Bayesian) t_f estimation. During future use of the Bayesian α -switching
 400 model, feature data may be provided to the model within only a single stage of crack growth. To prevent
 401 the model from falsely selecting an α switch-point and separating model parameters, the uniformity
 402 and convergence of α_{sp} can be evaluated to motivate the selection of the number of switch-points (if
 403 any). Beyond the FFM, the identification of switch-points may be useful in analyzing data through
 404 conventional analysis such as Paris Law; segmenting the data allows more accurate characterization of
 405 the different stages.

Table 4: Parameters of the α -switching Bayesian model (real data)

Parameter	Prior
t_f	Improper uniform distribution with lower bound of t
k_1	Improper uniform distribution with lower bound of 0
k_2	Improper uniform distribution with lower bound of 0
α_1	Uniform distribution between 1.5 and 2.5
α_2	Uniform distribution between 2.0 and 2.2
α_{sp}	Uniform distribution between 0 and t
σ_l	Half normal distribution, standard deviation of 0.8

406 5 Summary and Conclusions

407 When limited data are available for analysis, future events can be difficult to accurately predict.
 408 For failure events (t_f) which exhibit positive feedback failure mechanisms, the failure forecast method
 409 (FFM) allows for t_f predictions made using a single measured feature, unaffected by application specific
 410 experimental parameters and their uncertainty. Classically, the FFM implementation assumes linearity
 411 of the inverse feature rate, and creates a single estimation of t_f from a single realization of data from
 412 linear regression. Assuming the inverse feature rate's linearity causes a rigidity in the FFM because the
 413 governing phenomena often exhibit nonlinear inverse feature rate behavior, which has been observed in
 414 early and late stage crack growth [15, 16]. In this paper, we developed a Bayesian statistical model
 415 which relaxes this linearity assumption, and samples the posterior distribution of t_f , allowing for the
 416 generation of probability distributions for t_f .

417 For the specific application of fatigue crack growth, t_f (Bayesian) was compared against a
 418 statistical model of the "classic" FFM implementation, t_f (regression). We first compared the two
 419 models on synthetic data based on a real accelerated fatigue test published in [24], and then compared
 420 both models' t_f estimation made by the models on an unaltered accelerated fatigue test from [34].

421 In the study performed with synthetic data, t_f (Bayesian) was able to accurately converge to
 422 t_f estimation to the true t_f values for $\alpha = \{1.75, 2.0, 2.25\}$ across all noise levels, while the linear
 423 regression model was only able to converge to the correct t_f for data generated with $\alpha = 2.0$ across
 424 all noise levels. t_f estimation results of this study are shown in figures (5) and (6). The Bayesian
 425 model behaved mostly independent of the true α value of each synthetic data simulation, save for slight

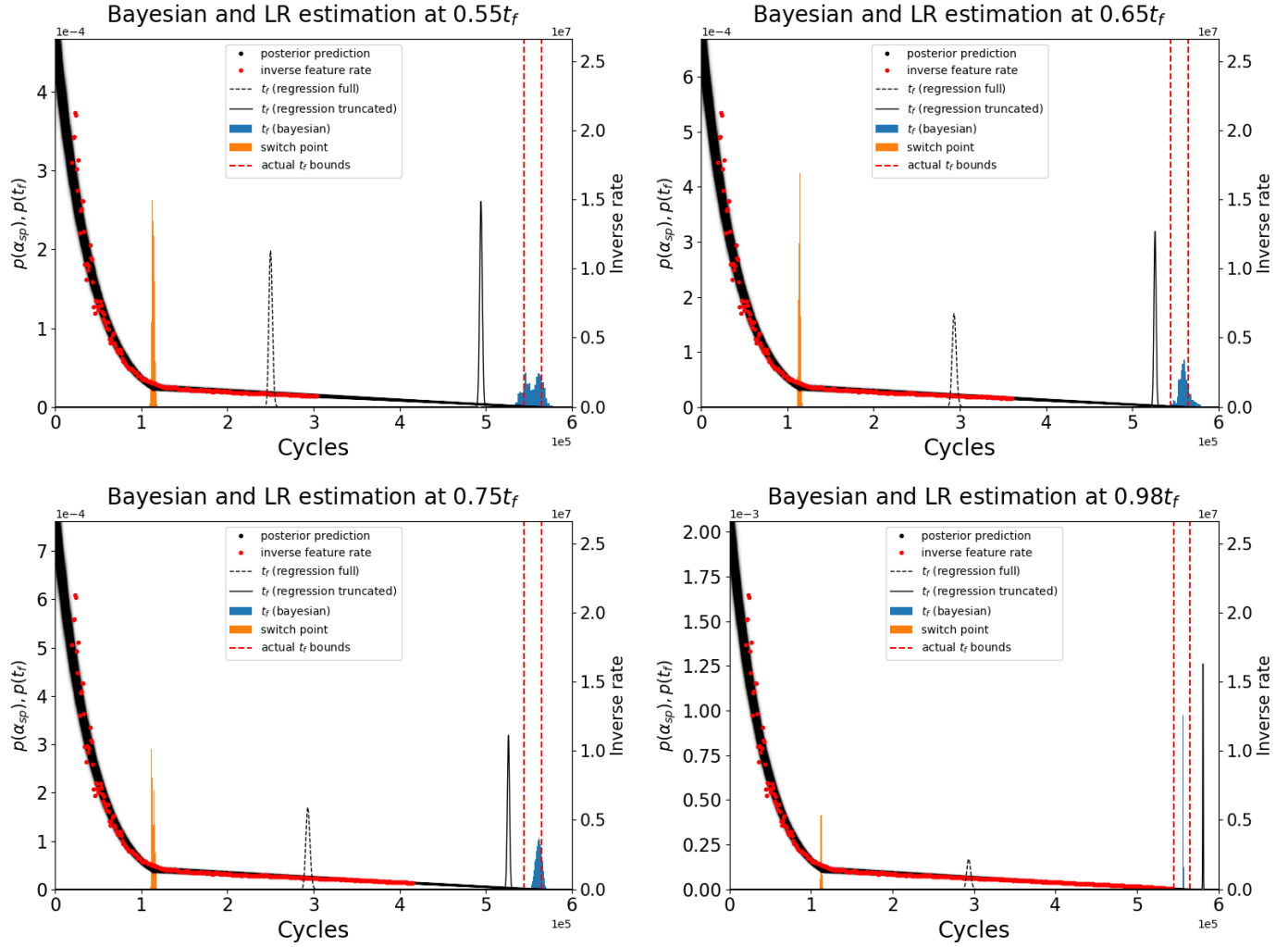


Figure 8: Results from using the α -switching Bayesian model and linear regression model on data from a real un-altered fatigue test for cycle predictions $0.55t_f$ - $0.98t_f$. Black shaded regions show the posterior prediction, orange regions show the posterior distribution of α_{sp} , blue regions show the t_f (Bayesian) posterior distribution, dashed and solid black lines show the t_f (regression) distribution for non-truncated data and truncated data, respectively. Inverse feature rate data is shown in red dots, and the range of actual t_f is shown in dashed red lines. Primary y-axis has units of probability density for distributions $p(\alpha_{sp})$ and $p(t_f)$, and secondary axis has units of inverse feature rate for experimental data and Bayesian posterior predictive.

426 increase in t_f distribution spread as the α value increased. The t_f (Bayesian) estimations across all α
 427 levels developed a negative bias at cycles $0.4t_f - 0.6t_f$, provided a positive bias at cycle $0.7t_f$, before
 428 converging to the true t_f value at cycles $0.8t_f$ and $0.9t_f$. The amount of bias was proportional to the
 429 level of noise. Joint distributions of sampled variables $t_f-\alpha$ in the Bayesian model also exhibited the
 430 same trend for all α values; these variables were observed to be highly negatively correlated.

431 The t_f estimations from both models were also compared on data from an un-altered fatigue
 432 test from [34]. To account for the non-stationarity often observed in the inverse feature rate data, the
 433 Bayesian model was adapted to incorporate an α switch point, allowing for two sets of Θ (Bayesian
 434 model parameters) to be sampled before and after the α switch point. The α -switching Bayesian model
 435 was able to accurately estimate t_f for cycles $0.55t_f$ onward, by effectively sampling the transition point
 436 α_{sp} and truncating the data after stage 1 crack growth, which was predicted to occur approximately
 437 20% through the fatigue experiment. The α -switching Bayesian model was also used to estimate a
 438 truncation point for the linear regression model, which performed much more accurately when using
 439 data only after α_{sp} .

440 The benefits of truncating the early stage crack growth motivates future work which explores the
 441 benefits of windowing data, impacting the t_f for both models. Some discussion is presented in [23],
 442 regarding windowing feature data for the linear regression model, but there is no work exploring the
 443 effects on the Bayesian model of windowing data.

444 As seen in figure (6), the Bayesian model showed a very high negative correlation between t_f and
 445 α . This result also motivates future iterations of the Bayesian model which accounts for this correlation
 446 by establishing jointly distributed t_f and α parameters, or simplifying the model based on principal
 447 component analysis.

448 Acknowledgements

449 The U.S.A. authors acknowledge support for this work was provided by the University of Dayton
 450 on subcontract FA8650-16-D-0311 under master contract with Air Force Research Laboratory/Eglin
 451 Air Force Base. The U.K. authors acknowledge support from the UK Engineering and Physical Sciences
 452 Research Council via the UK Research Centre in NDE, EP/L022125/1.

453 References

- 454 [1] C. R. Farrar and K. Worden, “An introduction to structural health monitoring.,” Philosophical
 455 Transactions. Series A, Mathematical, Physical, and Engineering Sciences, 2007.
- 456 [2] N. Chen and K. L. Tsui, “Condition monitoring and remaining useful life prediction using
 457 degradation signals: revisited,” IIE Transactions, vol. 45, pp. 939–952, sep 2013.
- 458 [3] X.-S. Si, W. Wang, C.-H. Hu, D.-H. Zhou, and M. G. Pecht, “Remaining useful life estimation
 459 based on a nonlinear diffusion degradation process,” IEEE Transactions on Reliability, vol. 61,
 460 no. 1, pp. 50–67, 2012.

- 461 [4] S. K. Everton, M. Hirsch, P. Stravroulakis, R. K. Leach, and A. T. Clare, “Review of in-situ
462 process monitoring and in-situ metrology for metal additive manufacturing,” Materials & Design,
463 vol. 95, pp. 431–445, 2016.
- 464 [5] P. Paris and F. Erdogan, “A critical analysis of crack propagation laws,” ASME Journal of Basic
465 Engineering, vol. 85, no. 1, pp. 528–534, 1963.
- 466 [6] X.-S. Si, W. Wang, C.-H. Hu, and D.-H. Zhou, “Remaining useful life estimation—a review on the
467 statistical data driven approaches,” European Journal of Operational Research, vol. 213, no. 1,
468 pp. 1–14, 2011.
- 469 [7] J. Z. Sikorska, M. Hodkiewicz, and L. Ma, “Prognostic modelling options for remaining useful life
470 estimation by industry,” Mechanical Systems and Signal Processing, vol. 25, no. 5, pp. 1803–1836,
471 2011.
- 472 [8] S. Beretta and M. Carboni, “Experiments and stochastic model for propagation lifetime of railway
473 axles,” Engineering fracture mechanics, vol. 73, no. 17, pp. 2627–2641, 2006.
- 474 [9] S. Beretta and A. Villa, “A RV approach for the analysis of fatigue crack growth with NASGRO
475 equation,” in 4th International ASRANAT Colloquium, pp. 1–7, 2008.
- 476 [10] C. Mallor, S. Calvo, J. L. Núñez, R. Rodríguez-Barrachina, and A. Landaberea, “Full second-order
477 approach for expected value and variance prediction of probabilistic fatigue crack growth life,”
478 International Journal of Fatigue, vol. 133, p. 105454, 2020.
- 479 [11] M. Jimenez-Martinez and M. Alfaro-Ponce, “Fatigue damage effect approach by artificial neural
480 network,” International Journal of Fatigue, vol. 124, pp. 42–47, 2019.
- 481 [12] J. F. Barbosa, J. A. F. O. Correia, R. C. S. F. Júnior, and A. M. P. De Jesus, “Fatigue life
482 prediction of metallic materials considering mean stress effects by means of an artificial neural
483 network,” International Journal of Fatigue, vol. 135, p. 105527, 2020.
- 484 [13] T. FUKUZONO, “A new method for predicting the failure time of a slope,” in Proceedings of 4th
485 International Conference and Field Workshop on Landslide., 1985, pp. 145–150, 1985.
- 486 [14] B. Voight, “A method for prediction of volcanic eruptions,” Nature, 1988.
- 487 [15] B. Voight, “A relation to describe rate-dependent material failure,” Science, 1989.
- 488 [16] R. R. Cornelius and P. A. Scott, “A materials failure relation of accelerating creep as empirical
489 description of damage accumulation,” Rock Mechanics and Rock Engineering, vol. 26, no. 3,
490 pp. 233–252, 1993.
- 491 [17] R. R. Cornelius and B. Voight, “Seismological aspects of the 1989–1990 eruption at Redoubt
492 Volcano, Alaska: The Materials Failure Forecast Method (FFM) with RSAM and SSAM seismic
493 data,” Journal of Volcanology and Geothermal Research, vol. 62, no. 1-4, pp. 469–498, 1994.

- 494 [18] R. R. Cornelius and B. Voight, “Graphical and PC-software analysis of volcano eruption precursors according to the Materials Failure Forecast Method (FFM),” Journal of Volcanology and Geothermal Research, vol. 64, no. 3-4, pp. 295–320, 1995.
- 497 [19] G. B. Crosta and F. Agliardi, “Failure forecast for large rock slides by surface displacement measurements,” Canadian Geotechnical Journal, vol. 40, no. 1, pp. 176–191, 2003.
- 499 [20] A. Boue, P. Lesage, G. Cortés, B. Valette, and G. Reyes-Dávila, “Real-time eruption forecasting using the material Failure Forecast Method with a Bayesian approach,” Journal of Geophysical Research: Solid Earth, vol. 120, no. 4, pp. 2143–2161, 2015.
- 502 [21] Y. Lavallée, P. G. Meredith, D. B. Dingwell, K.-U. Hess, J. Wassermann, B. Cordonnier, A. Gerik, and J. H. Kruhl, “Seismogenic lavas and explosive eruption forecasting,” Nature, vol. 453, no. 7194, p. 507, 2008.
- 505 [22] J. Corcoran, “Rate-based structural health monitoring using permanently installed sensors,” Proc. R. Soc. A, vol. 473, no. 2205, p. 20170270, 2017.
- 507 [23] M. D. Todd, M. Leung, and J. Corcoran, “A probability density function for uncertainty quantification in the failure forecast method,” in Proceedings of the 9th European Workshop on Structural Health Monitoring, Manchester, UK July, pp. 9–11, 2018.
- 510 [24] M. S. H. Leung, J. Corcoran, P. Cawley, and M. D. Todd, “Evaluating the use of rate-based monitoring for improved fatigue remnant life predictions,” International Journal of Fatigue, vol. 120, pp. 162–174, 2019.
- 513 [25] A. F. Bell, M. Naylor, M. J. Heap, and I. G. Main, “Forecasting volcanic eruptions and other material failure phenomena: An evaluation of the failure forecast method,” Geophysical Research Letters, 2011.
- 516 [26] A. Bevilacqua, E. B. Pitman, A. Patra, A. Neri, and M. Bursik, “Probabilistic Enhancement of the Failure Forecast Method Using a Stochastic Differential Equation and Application to Volcanic Eruption Forecasts,” Frontiers in Earth Science, 2019.
- 519 [27] A. Boue, P. Lesage, G. Cortés, B. Valette, G. Reyes-Dávila, R. Arámbula-Mendoza, and A. Budi-Santoso, “Performance of the ‘material Failure Forecast Method’ in real-time situations: A Bayesian approach applied on effusive and explosive eruptions,” Journal of Volcanology and Geothermal Research, vol. 327, pp. 622–633, 2016.
- 523 [28] A. F. Bell, M. Naylor, and I. G. Main, “The limits of predictability of volcanic eruptions from accelerating rates of earthquakes,” Geophysical Journal International, vol. 194, no. 3, pp. 1541–1553, 2013.
- 526 [29] D. V. Hinkley, “On the ratio of two correlated normal random variables,” Biometrika, vol. 56, no. 3, pp. 635–639, 1969.
- 527

- 528 [30] A. Gelman, H. S. Stern, J. B. Carlin, D. B. Dunson, A. Vehtari, and D. B. Rubin,
529 Bayesian Data Analysis. Chapman and Hall/CRC, 2013.
- 530 [31] A. Gelman, D. Simpson, and M. Betancourt, “The prior can often only be understood in the
531 context of the likelihood,” Entropy, vol. 19, no. 10, p. 555, 2017.
- 532 [32] J. Salvatier, T. V. Wiecki, and C. Fonnesbeck, “Probabilistic programming in Python using
533 PyMC3,” PeerJ Computer Science, vol. 2, p. e55, 2016.
- 534 [33] M. D. Hoffman and A. Gelman, “The No-U-turn sampler: adaptively setting path lengths in
535 Hamiltonian Monte Carlo,” Journal of Machine Learning Research, vol. 15, no. 1, pp. 1593–1623,
536 2014.
- 537 [34] J. Corcoran, C. M. Davies, P. Cawley, and P. B. Nagy, “A Quasi-DC Potential Drop Measurement
538 System for Material Testing,” IEEE Transactions on Instrumentation and Measurement, vol. 69,
539 no. 4, pp. 1313–1326, 2019.